Hindawi
Mathematical Problems in Engineering
Volume 2022, Article ID 7891232, 14 pages
https://doi.org/10.1155/2022/7891232

Research Article

Analysis of Vehicle-Pedestrian Accident Risk Based on Simulation Experiments

Rui Cheng,[1] **Ye Pan**,[1] **and Lian Xie**[1,2]

[1]*Key Laboratory of ITS (Guilin University of Electronic Technology), Education Department of Guangxi Zhuang Autonomous Region, Guilin 541004, China*
[2]*Intelligent Transportation Systems Research Center, Wuhan University of Technology, Wuhan 430063, China*

Correspondence should be addressed to Lian Xie; xielian@whut.edu.cn

Received 16 May 2022; Revised 16 July 2022; Accepted 4 August 2022; Published 29 August 2022

Academic Editor: Meng Li

Vehicle-pedestrian accidents are one of the main types of road traffic accidents in China because of their mixed traffic features. By analyzing the characteristics of vehicle-pedestrian accidents, the head injury criterion (HIC) was selected as a quantitative index of pedestrian head injury risk, and vehicle-pedestrian collision simulation tests were carried out using PC-Crash. From the collected test data, the multivariate relationship models between the HIC, vehicle speed, and collision angle were fitted for different vehicle types. A risk assessment method for vehicle-pedestrian accidents based on the HIC was proposed by the Fisher optimal segmentation algorithm. Finally, a new index for evaluating the accuracy of accident risk classification, the degree of error classification, was proposed to verify the validity of the accident risk assessment method. The results show that vehicle speed, collision angle, and vehicle type play a key role in pedestrian injury. Flat-headed vehicles are more likely to cause head injuries to pedestrians than high-headed and low-headed vehicles. Rear-end collisions cause more injuries to pedestrians than side collisions. The research results can provide guidance and a basis for accident liability determination, speed limit management, vehicle safety design, and human injury mechanism analysis.

1. Introduction

With the rapid growth of the social economy and the continuous innovation of science and technology, automobile manufacturers are increasingly pursuing comfort, safety, and environmental protection, as well as the protection of passengers in vehicles, while their awareness of the protection of pedestrians outside vehicles is relatively weak. Among all road traffic participants, pedestrians are one of the most vulnerable groups. In recent years, the lack of safety awareness of drivers and pedestrians in observing traffic rules and poor traffic management has caused frequent pedestrian traffic accidents, and the resulting losses are difficult to estimate. According to statistics in China's annual statistical report of road traffic accidents (2021), pedestrian traffic accidents accounted for approximately 21% of all accidents in the whole year but lead to approximately 27% mortality [1]. The reason is that road traffic in China is mainly typical plane cross-mixed traffic. Although most urban roads are divided into nonlane isolation facilities, collision accidents between cars and pedestrians cannot be eliminated.

The USA and the European Union began to pay attention to pedestrian safety in the mid-1970s. Since then, biological samples and mechanical dummies have been used to carry out real vehicle test studies instead of pedestrians, including human injury evaluation, the impact of overall vehicle structure design on pedestrian injury, and human injury prevention measures and safety countermeasures [2–5]. For example, Severy et al. used mechanical dummies to study vehicle-pedestrian collision accidents successively in 1963 and 1966, which was the first experiment in this field [6]. On this basis, other relevant scholars used dummies or corpses to conduct a series of experiments under different collision conditions. The data obtained from a test are fitted using mathematical regression with different methods to obtain a corresponding empirical formula [7].

Due to the high cost of real vehicle tests and considering the feasibility of computer technology simulation, some scholars have developed mature accident reconstruction software (SMAC, AUTOSMAC, PC-Crash, etc.) by building digital dummy models, providing another way to analyze and study vehicle-pedestrian collision accidents [8]. A dummy model should not only adapt to human body dynamics analysis but also be able to carry out human body damage analysis [9, 10]. Therefore, a digital dummy should have high computational efficiency, be able to adapt to different environments, conform to various biomechanical characteristics of the human body, and output corresponding parameter information for the calculation of a damage index.

For example, Xu et al. proposed a personalized customization method to divide the pedestrian structure into independent modules according to obvious bone markers and establish a multibody model and a finite element (FE) model for each independent module to form a hybrid pedestrian model [11]. To characterize the complex vehicle-pedestrian interaction process, Grindle et al. developed and validated a detailed pedestrian FE model corresponding to 50% male to predict injuries caused by pedestrian accidents. Compared with a simplified pedestrian model, the constructed model shows higher biofidelity [12]. In addition, to explore the damage prediction ability of the Total Human Body Model for Safety (THUMS) finite element human model (FE-HBM) in real-world vehicle-pedestrian collisions, Panday et al. used sequences of multibody tools and finite element tools to reconstruct 10 vehicle-pedestrian crashes with lower limb injuries. The conclusion shows that the THUMS FE-HBM can better predict pedestrian injuries in real traffic accidents [13]. Lalwala et al. also reconstructed a THUMS pedestrian model using pedestrian accident cases. It can be observed from the reconstruction study that the kinematic response and damage response of their THUMS lower limb model are in good agreement with the actual collision data [14].

With the continuous improvement of accident databases by traffic research institutions in various countries, in recent years, some scholars have relied on cases in a database to explore the significant cause factors affecting the frequency and severity of vehicle-pedestrian accidents. For example, in terms of road control, based on three years of traffic accident data in Hong Kong, Zhu selected the best performance artificial neural network (ANN) model by comparing various data mining algorithms and determined the most significant factors causing fatal and serious accidents. The results show that in rainy weather, fatal and serious vehicle-pedestrian collisions are more likely to occur in the case of intersection signal failures [15]. Sheykhfard et al. used a structural equation model (SEM) to investigate the data of 1358 pedestrian accidents in Gilan Province, Iran, from 2012 to 2018. Factor analysis results showed that the quality defects of automobiles and poor traffic design at intersections, major urban roads, and outer ring roads are important reasons for the increase in fatal accidents [16]. With the continuous improvement of research methods, Kamboozia et al. constructed a pedestrian accident severity prediction model using ANNs and multiple logistic regression. By comparing the severity prediction results of pedestrian accidents using different methods, they put forward the best prevention and control measures to improve pedestrian safety on rural roads [17].

In terms of vehicle and pedestrian characteristics, Park et al. used a multilevel model to investigate the differences between the low-level individual characteristics and high-level community environmental characteristics of pedestrian collisions in Seoul, South Korea. The results showed that older pedestrians suffered more serious pedestrian injuries; trucks and vans were more likely to cause serious pedestrian injuries [18]. While researching the influence of alcohol, Lasota's survey found that younger victims were more likely to die at the scene of an accident, especially in rural areas [19].

To determine the high-risk and low-risk areas of pedestrian death accidents in Iran, Hasani et al. input collected pedestrian accident data into ArcGIS software to identify high-risk and low-risk areas by calculating the spatial autocorrelation of the data [20]. Jamali-dolatabad et al. collected pedestrian traffic accident data in Tabriz from 2014 to 2015, with fatal accidents as the case group and nonfatal accidents as the control group. Their results showed that the significantly related factors influencing pedestrian death were pedestrian age, type of license plate, accident season, type of driving license, gender of pedestrian, and pedestrian fault [21]. Feng et al. used a multivariate logistic regression model to analyze 111 collision accidents and found that collision with the front windshield frame usually leads to more serious damage. When the collision speed exceeds 40 km/h, the risk of serious head injury for pedestrians increases sharply [22]. While discussing the characteristics of fatal pedestrian accidents involving low-speed vehicles, Matsui, a Japanese scholar, thought the relative percentage of pedestrian deaths is significantly higher when vehicles are traveling at low speeds, except for accidents involving box trucks or SUVs [23].

At present, researchers mainly carry out vehicle-pedestrian accident research through simulation and accident case statistical analysis. In terms of simulation, most existing studies are optimized and improved for a dummy model, and few involve the risk assessment of pedestrian accidents by developed dummy models. However, an accident risk assessment based on the statistical analysis of accident cases mainly considers macro factors, such as vehicle speed, vehicle type, accident environment, and road design, but lacks in-depth discussion of the impact of micro-factors (such as pedestrian speed, collision angle, type of head, and pedestrian and vehicle lateral contact position) on human injuries. Therefore, this paper adopts computer simulation technology to carry out a risk analysis of vehicle-pedestrian accidents with a more mature multirigid body dummy model. Common computer simulation software for accident reappearance includes SMAC and AUTOSMAC, developed by the National Road Traffic Safety Administration of the USA, and PC-Crash, developed by the DSD of Austria. Since SMAC and AUTOSMAC cannot realize pedestrian collision simulation, PC-Crash has been constantly updated and

upgraded, adding pedestrian multirigid body and FE calculation models on the basis of a single rigid body model, which has been widely recognized in the field of road traffic accident reconstruction and has become the most widely used accident simulation software. In view of this, this paper chooses PC-Crash to carry out simulation tests. Through the investigation and analysis of accident cases, the typical collision patterns of vehicle-pedestrian traffic accidents are determined. Based on a rigid body dynamics method, PC-Crash is utilized to build three vehicle rigid body models (short head, high head, and flat head) and a pedestrian multirigid body model, HTC is used to measure the risk of pedestrian head injuries, a vehicle-pedestrian collision simulation test is carried out under the influence of different vehicle types, vehicle speeds, pedestrian speeds, collision angles, and relative collision positions, and the influence of multiple factors on pedestrian injury is studied. According to the collected test data, the relationship model between the HIC and vehicle speed under different collision angles is fitted using multiple regression analysis for different vehicle models. A reasonable evaluation series and corresponding HIC threshold of pedestrian injury risk in vehicle-pedestrian accidents are determined using the Fisher optimal segmentation algorithm, and the vehicle-pedestrian accident risk evaluation method based on HIC is given. Compared with risk assessment based on accident case analysis, the research results obtained by simulation in this paper are not affected by factors, such as region, time, and traffic characteristics, and have universal applicability.

2. Characteristics Analysis of Vehicle-Pedestrian Collision Accidents

2.1. Collision Form. Compared with people in a vehicle, pedestrians are completely exposed to the external environment, have strong subjective randomness when walking, and choose the road, direction, and walking speed that they think will reach their destination. The characteristics of pedestrian traffic are related to the height, age, psychology, physique, and gender of pedestrians, which leads to the diversity and complexity of vehicle-pedestrian collision accident patterns and makes them face different injury risks.

There are three common collision patterns between cars and pedestrians: front, side, and rear collisions with pedestrians. Because frontal collisions between vehicles and pedestrians occur most frequently and are most likely to lead to pedestrian deaths, this paper focuses on frontal collisions between vehicles and pedestrians. This collision process can be divided into three stages, as shown in Figure 1.

① Collision phase: The pedestrian's lower limbs first collide with the front part of the vehicle. As the vehicle continues to move forward, the pedestrian's chest and abdomen contact and collide with the engine hood of the vehicle. If the vehicle speed is high, the pedestrian's head will collide with the front windshield or A-pillar of the vehicle. Usually, at this stage, pedestrians are subjected to a large impact force, resulting in very serious pedestrian damage. ② Flight phase: After the collision, the human body continues to fly in the air. At this stage, the pedestrian does not contact any object and only receives friction resistance from the air. ③ Landing and rolling stage: After falling to the ground, pedestrians are affected by the friction resistance of the road and immediately begin to slow down. According to the different falling speeds and directions, the pedestrian experiences a composite motion state of sliding, rolling, or rotating on the road surface.

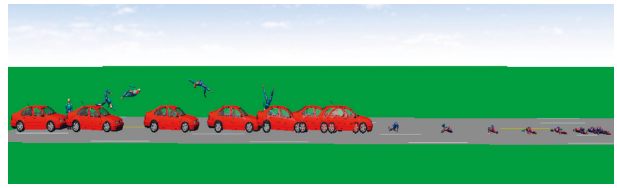

Figure 1: Diagram of the collision process.

2.2. Pedestrian Injury Mechanism. In vehicle-pedestrian collision accidents, the injuries suffered by pedestrians can be roughly divided into two categories, namely, primary injuries and secondary injuries. A primary injury refers to an injury caused by the first collision or crushing of the human body between a vehicle and a pedestrian. A secondary injury refers to an injury caused by the collision and scraping between the human body and the ground or other objects after being hit. Generally, pedestrian injury mechanisms can be divided into the following two categories according to different vehicle types:

(1) When a pedestrian collides with a high-head vehicle (such as an off-road vehicle) or a low-head vehicle (such as a car), because the front collision contact point of the vehicle is not higher than the center of gravity of the human body, the first damage to the human body is the car's front bumper, engine cover, and front windshield contact collision with the human body. The second collision is the human body in the air after the overturn of the vehicle, subsequent contact collision or landing, and road impact causing damage.

(2) When a pedestrian collides with a flat-headed vehicle (such as a van or truck), the height of the front part of the vehicle is higher than the height of the pedestrian's center of gravity, and the pedestrian's legs, torso, or even their whole body contact with the front part of the vehicle, resulting in a large contact surface and easily causing nonobvious trauma to the human body but especially serious internal injuries. After the collision, the human body experiences a flat throwing movement, which will cause obvious falling injury and then scratching or rolling.

According to the statistical analysis results of pedestrian traffic accidents in China [24], Figures 2 and 3 show the injury frequency of pedestrian body parts and the distribution frequency of fatal body parts, respectively. Figure 2 shows that the most vulnerable parts are people's legs and head, among which leg injuries account for 40%, and 32% of pedestrians suffer head injuries. Figure 3 shows that head and chest injuries are the main causes of pedestrian deaths,

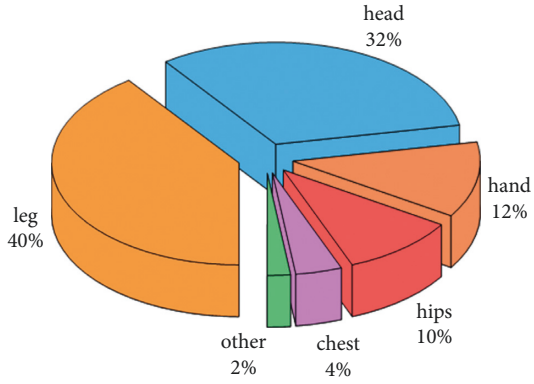

Figure 2: Distribution of pedestrian injuries.

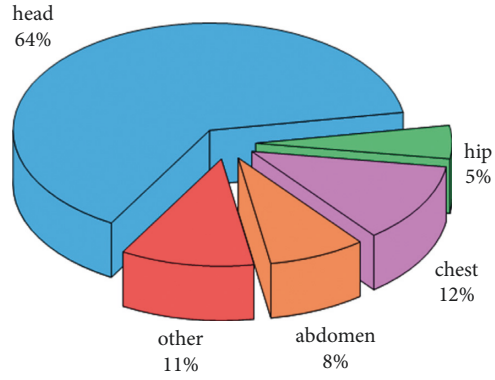

Figure 3: Distribution of fatal pedestrian parts due to injury.

accounting for 64% and 12%, respectively. Therefore, the analysis and protection of head injuries play an important role in pedestrian safety research.

3. Evaluation Standard and Method of Head Injury

3.1. Head Injury Criterion. The head injury evaluation standard is defined by physical parameters related to injury intensity or a function composed of several physical parameters, which is related to the degree of risk of a certain part of the human body being damaged and is used to measure whether the load exceeds the degree of causing a certain injury. At present, the head injury criterion (HIC) proposed by Versace in 1971 is widely adopted internationally, serves as the basis of the Federal Motor Vehicle Safety Standards (FMVSS), and is used to evaluate vehicle safety. In domestic and foreign laws and standards, the HIC has become the most extensively employed criterion for evaluating head injuries. The safety limit value for the HIC is generally 1,000. According to related statistics, when the HIC > 1,000, the probability of fatal head fracture exceeds 33%. Its calculation formula is as follows [25]:

$$\mathrm{HIC} = \left[(t_2 - t_1)\left(\frac{1}{t_2 - t_1}\int_{t_1}^{t_2} a(t)\mathrm{d}t\right)^{2.5}\right]_{\max} \quad (1)$$

where a represents the resultant acceleration at the center of gravity of the head in a collision; t_1 and t_2 are two different times during the collision, which are chosen to maximize the HIC; and $1/t_2 - t_1 \int_{t_1}^{t_2} a_t \mathrm{d}t$ represents the average resultant acceleration between t_1 and t_2. The time interval (i.e., from t_1 to t_2) of the HIC substantially affects the calculation of its value. Thus, this paper selects 15 ms, as adopted by the U-NCAP collision test.

3.2. Fisher Optimal Segmentation Method. When the HIC > 1,000, head injuries tend to be more severe, but there is no clear standard for using the HIC to measure the severity of head injuries. Therefore, this paper uses the Fisher optimal segmentation algorithm to classify the HIC data obtained from a simulation test to obtain a pedestrian accident risk classification scheme, including the optimal classification number and corresponding index thresholds of each level. The principle of Fisher optimal segmentation is to ensure the ordered sample data of each group after segmentation and minimize the sum of squares of deviations within the group. In this case, the corresponding grouping is the optimal segmentation. The specific implementation method is described below [26].

3.2.1. Define and Calculate the Class Diameter. The Fisher optimal segmentation algorithm usually uses the diameter to define the difference degree in a class. When the difference degree in the class is smaller, the class diameter is smaller, indicating that the sample attributes in the class tend to be consistent. If the data samples are divided into k categories and have C_{m-1}^{k-1} classification methods, assuming that H_{ij} is one of the classifications, then the sample data contained in the classification are denoted as $\{x_i, x_{i+1}, \ldots, x_j\}$ $(1 \le i < j)$. The sum of the squares of deviations of the samples in H_{ij} is defined as the class diameter $D(i, j)$, namely,

$$D(i, j) = \sum_{i=1}^{j} \left(x_i - \overline{x}_{ij}\right)^T \left(x_i - \overline{x}_{ij}\right), \quad (2)$$

where x_i is the standardized sample value and $\overline{x}_{ij}$ is the average value from sample i to sample j.

3.2.2. Calculate the Classification Error Function. Generally, an error function is used to define the merits and demerits of data sample classification. If m data samples are divided into k categories, the corresponding error function of this category is

$$e[p(m, k)] = \sum_{\eta=1}^{k} D\left(i_\eta, i_{\eta+1} - 1\right). \quad (3)$$

That is, the error function of any classification method is expressed as the sum of all diameters. The smaller $e[p(m, k)]$ is, the smaller the sum of diameters of all classifications is, and the better the classification effect is.

3.2.3. Determine the Optimal Solution. According to formula (3), when $k = 2$, the error function corresponding to the optimal 2 classifications is

$$e[p(m,2)] = \min_{2\le i\le m}\{D(1,i-1) + D(i,m)\}. \quad (4)$$

When $k>2$, the error function corresponding to the optimal k classification is

$$e[p(m,k)] = \min_{2\le i\le m}\{e[p(i-1,k-1)] + D(i,m)\}, \quad (5)$$

Here, it is necessary to determine the appropriate classification point i_k guarantee formula (5) to calculate the minimum value, that is, $e[p(m,k)] = e[p(i_k-1,k-1)] + D(i_k,m)$ is the minimum, so the k class $H_k = \{i_k, i_{k+1}, \ldots, m\}$ can be obtained. Then, the classification point $i_{k\text{-}1}$ is determined to make it satisfy $e[p(i_k-1,k-1)] = e[p(i_{k-1}-1,k-2)] + D(i_{k-1},i_k-1)$ so that the k–1 class $H_{k-1} = \{i_{k-1}, i_{k-1}+1, \ldots, i_k-1\}$ can be obtained, all the classifications $H_1, H_2, \ldots, H_k$ can be obtained by analogy, and finally, the optimal solution can be obtained.

3.2.4. Determine the Optimal Classification Number. Generally, the optimal classification is determined by drawing the curve of the minimum error function changing with the classification number k. When the curve curvature changes significantly, the corresponding k value is the appropriate classification number. In addition, to determine the k value more accurately, the minimum error function ratio $\beta(k)$ between adjacent classification numbers can be further calculated. The larger $\beta(k)$ is, the better the classification effect is, as shown in

$$\beta(k) = \frac{e[p(m,k)]}{e[p(m,k+1)]}. \quad (6)$$

3.3. Abbreviated Injury Scale. In addition, to standardize the evaluation of injury levels after accidents, countries around the world have put forward the abbreviated injury scale (AIS) to evaluate the risk of injury after years of accident research. The AIS is a scoring method for classifying trauma based on anatomical indexes. It defines nine anatomical ranges to determine the location of trauma, specifically including head (skull and brain), face (eyes and ears), neck, chest, abdominal and pelvic organs, spine (cervical spine, thoracic spine, and lumbar spine), upper limbs, lower limbs, pelvis and buttocks, body surface (skin) and thermal injury, and other injuries. According to the pedestrian injury report, the trauma level of the pedestrian after the accident was assessed with six grades, as shown in Table 1.

4. Data Collection

4.1. Test Scenario. First, a two-way four-lane road model with a lane width of 3.5 m, total length of 100 m, and pavement adhesion coefficient of 0.7 is constructed using PC-Crash, as shown in Figure 4. Then, the software's human body model is used. The model is a multibody dynamic system consisting of 16 independent rigid bodies and 15 hinge joints, as shown in Figure 5. Each part of the human body (head, trunk, limbs, buttocks, etc.) is regarded as an independent rigid body, and its surface shape is defined by an ellipsoid, which simplifies the joint of each part to a hinge connection. In this paper, adult males were selected as the research object, and multiple rigid body model parameters were assigned according to physical characteristics. The specific setting parameters are shown in Table 2.

Table 1: AIS classification standard.

AIS score	Description	Mortality rate (%)
1	Mild	0.6
2	Moderate	3.2
3	Heavy	9.3
4	Severe	28.3
5	Critical	78.4
6	Extreme (currently incurable)	100

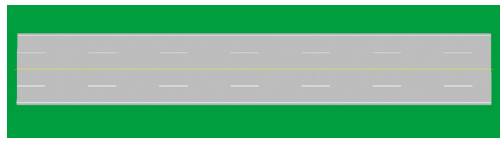

Figure 4: Road scenario.

According to the analysis in Section 2.2, a Volkswagen Bora 2.0, Audi Q5 2.0TDI, and Volkswagen T4 2.5 TDI (as shown in Figure 6) were selected from the PC-Crash database as representative models of low-head, high-head, and flat-head vehicles, respectively, to explore the impact of different head types on pedestrian injury risk.

4.2. Test Scheme. Considering that pedestrian speed may affect accident risk, this research carries out vehicle-pedestrian collision simulation tests under a pedestrian moving state. According to the statistical analysis of pedestrian motion state and collision angle in vehicle-pedestrian accidents in the literature [27], 55% of pedestrians are in a walking state, 38% are in a running state, and 4% are in a stationary state. The proportion of pedestrians in the lateral position (i.e., the walking direction of pedestrians is 90° from the driving direction of vehicles) is 68%, followed by the rear position (i.e., the walking direction of pedestrians is 0° from the driving direction of vehicles) and the facing position (i.e., the walking direction of pedestrians is 180° from the driving direction of vehicles), accounting for 21% and 7%, respectively. Therefore, this research chooses two states of walking and jogging for pedestrians (corresponding to a walking speed of adult males being approximately 5 km/h and a jogging speed being approximately 10 km/h), and the two orientations of collision angle between pedestrians and cars are 90° and 0° for experiments. In addition, to explore the impact of pedestrian collision position relative to vehicle on accident risk, this study selects the front 1/4 and 1/2 positions as research variables. Figure 7 shows the collision position of pedestrians relative to cars at different collision angles.

Considering the demands of road traffic car speed in China, at the same time to make the research more reasonable, the car speed is set to $V_S \in \{20, 30, 40, 50, 60, 70, 80, 90, 100, 110\}$ km/h. Combined with the analysis of the above

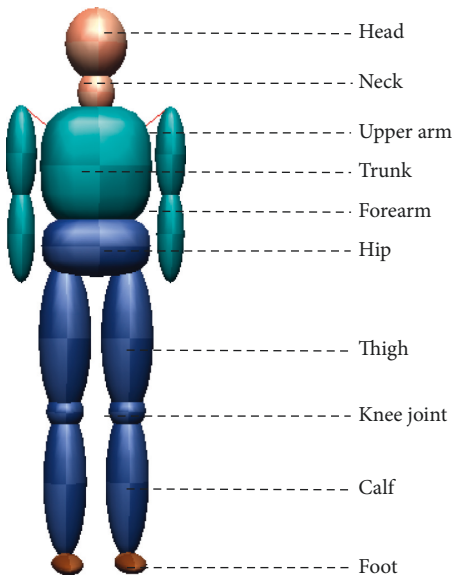

Figure 5: Pedestrian multibody model.

Table 2: Body parameters of 90th percentile adult males aged 18–60 years in China.

Height (mm)	Weight (kg)	Upper arm length (mm)	Forearm length (mm)	Thigh length (mm)	Calf length (mm)
1754	71	333	253	496	396

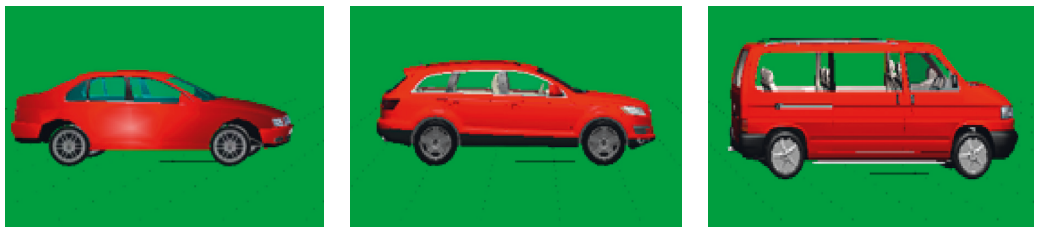

(a) (b) (c)

Figure 6: Test vehicle models. (a) VW Bora 2.0. (b) Audi Q5 2.0TDI. (c) VW T4 2.5 TDI.

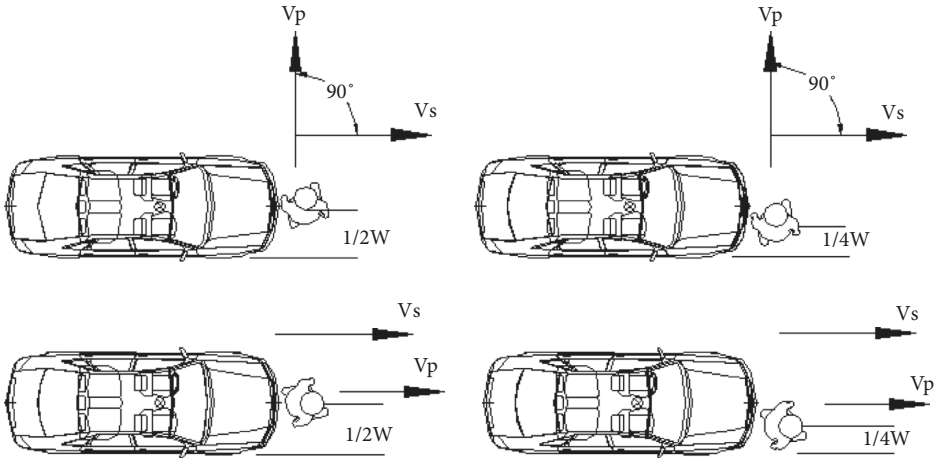

Figure 7: Diagram of the test collision location.

Table 3: Resultant head acceleration value of low-head vehicle and pedestrian collision (m/s^2).

Speed (km/h)	1/4W				1/2W			
	5 km/h		10 km/h		5 km/h		10 km/h	
	0°	90°	0°	90°	0°	90°	0°	90°
20	7325	4910	10743	5710	8893	5523	7418	5661
30	18432	8492	19722	5691	18817	7517	19366	5863
40	31446	10111	28788	12198	31143	7824	31050	9156
50	38902	16472	39020	12151	38179	17399	36127	11671
60	37538	19569	37202	20320	34151	26587	36897	17693
70	39112	29179	40570	25684	38536	32482	37900	32015
80	83079	57019	96861	46872	73810	36515	96522	30526
90	61532	70732	54079	52682	91077	58322	67637	48716
100	66272	70748	75818	58711	72905	54236	77429	35124
110	98648	73310	112221	75050	94712	55597	117232	60774

Table 4: Resultant head acceleration value of high-head vehicle and pedestrian collision (m/s^2).

Speed (km/h)	1/4W				1/2W			
	5 km/h		10 km/h		5 km/h		10 km/h	
	0°	90°	0°	90°	0°	90°	0°	90°
20	6850	6018	4975	3768	9324	4959	9367	4932
30	19676	6205	21291	5873	17794	8436	18627	5697
40	27784	10803	28913	11685	26035	11672	26990	10196
50	41633	17836	39939	14931	34615	16708	35541	13995
60	30945	22409	32566	16596	33216	24322	32900	17927
70	41164	27664	37652	24207	57948	33650	45046	23883
80	70486	32955	60383	31991	118726	37902	89432	37764
90	82572	54328	69229	38435	69090	53954	59607	45422
100	78490	57858	91205	51966	69118	54485	136390	64674
110	96015	64113	160570	84012	136823	54876	112009	54378

Table 5: Resultant head acceleration value of flat-head vehicle and pedestrian collision (m/s^2).

Speed (km/h)	1/4W				1/2W			
	5 km/h		10 km/h		5 km/h		10 km/h	
	0°	90°	0°	90°	0°	90°	0°	90°
20	72581	68028	57022	56185	102776	58738	96927	63485
30	55403	50536	65902	56045	93834	51304	77411	49532
40	63699	39733	84445	46869	76342	48448	86677	49439
50	78634	51023	103047	44617	115872	46188	102369	42441
60	115818	78840	130771	64405	152051	69207	147071	53681
70	130897	121951	168717	109352	157615	82202	171708	73181
80	154287	158591	144967	143215	207197	122008	206549	104993
90	152299	173736	147755	147764	183070	122477	177983	141675
100	282092	178430	244815	166398	264413	156806	260346	153319
110	375455	229065	418680	187684	430182	178198	448000	166874

variables, we set the model $M \in \{M_1, M_2, M_3\}$, wherein M_1, M_2, and M_3 represent the low-head, high-head, and flat-head vehicles, respectively; collision angle $\theta \in \{0°, 90°\}$; pedestrian walking speed $V_P \in \{5\,\text{km/h}, 10\,\text{km/h}\}$; collision position $R \in \{1/4\,W, 1/2\,W\}$, where W is the width of the front part of the car in meters. The simulation test involves 5 variables, namely, $\{M, \theta, V_S, V_P, R\}$. According to the values of each variable, a total of $3 \times 2 \times 10 \times 2 \times 2 = 240$ collision modes were simulated. Before the collision, the vehicle moves in a straight line, and after the collision, the vehicle is fully braked until it stops. The collision process is shown in Figure 1.

5. Results and Analysis

5.1. Model Fitting. Through each simulation test, the resultant acceleration value of the pedestrian head under different collision forms is obtained, as shown in Tables 3–5. The HIC value can be calculated using formula (1), as shown in Tables 6–8. Among them, the test data with a HIC value ≥ 1000 account for 75.8% of the total.

First, the Pearson correlation analysis between each variable and the HIC is carried out, and the results are listed in Table 9. ** in the table represents a significant

Table 6: HIC value of collision head between low-head vehicle and pedestrian.

	1/4W				1/2W			
Speed (km/h)	5 km/h		10 km/h		5 km/h		10 km/h	
	0°	90°	0°	90°	0°	90°	0°	90°
20	46	17	121	25	75	23	48	24
30	466	67	551	25	490	49	527	27
40	1770	104	1419	166	1728	55	1715	81
50	3013	352	3036	164	2875	403	2504	149
60	2756	541	2695	594	2176	1164	2640	420
70	3054	1468	3347	1067	2943	1920	2823	1851
80	20084	7837	29477	4802	14942	2572	29220	1644
90	9481	13432	6866	6431	25272	8293	12011	5288
100	11414	13440	15979	8432	14488	6916	16842	2334
110	30856	14690	42589	15577	27870	7358	47504	9192

Table 7: HIC value of collision head between high-head vehicle and pedestrian.

	1/4W				1/2W			
Speed (km/h)	5 km/h		10 km/h		5 km/h		10 km/h	
	0°	90°	0°	90°	0°	90°	0°	90°
20	39	28	18	9	85	17	86	17
30	548	31	668	27	426	66	478	25
40	1299	122	1435	149	1104	149	1208	106
50	3570	429	3218	275	2250	364	2404	234
60	1701	759	1932	358	2030	931	1982	434
70	3471	1285	2777	920	8160	2097	4348	890
80	13316	1990	9045	1848	49033	2823	24146	2798
90	19778	6945	12730	2924	12666	6826	8757	4439
100	17424	8129	25361	6215	12679	6995	69354	10738
110	28838	10507	104299	20653	69906	7122	42389	6961

Table 8: HIC value of collision head between flat-head vehicle and pedestrian.

	1/4W				1/2W			
Speed (km/h)	5 km/h		10 km/h		5 km/h		10 km/h	
	0°	90°	0°	90°	0°	90°	0°	90°
20	14327	12185	7838	7554	34185	8441	29527	10251
30	7294	5796	11255	7507	27228	6019	16832	5512
40	10338	3177	20919	4801	16256	5216	22329	5486
50	17504	5936	34412	4245	46139	4629	33848	3746
60	46085	17619	62430	10627	91011	12720	83740	6740
70	62581	52429	118035	39919	99565	19558	123337	14626
80	94393	101114	80777	78359	197276	52491	195738	36059
90	91382	127011	84717	84730	144763	52997	134915	76269
100	426669	135763	299372	114021	362929	98293	349136	92919
110	871989	253521	1145038	154059	1225307	135322	1356163	114839

Table 9: Correlation analysis.

	Vehicle speed	Collision position	Pedestrian speed	Collision angle	Vehicle type
HIC	0.333**	0.017	0.005	−0.181**	0.311**

correlation at a level of 0.01 (two-tailed test). The vehicle speed, collision angle, and vehicle type are significantly correlated with the HIC, while the collision position and pedestrian speed show a weak correlation. The analysis shows that the impact force of any part of the front of the vehicle on the pedestrian is equivalent, and the pedestrian speed relative to the vehicle speed can be ignored at the moment of collision. The above reasons lead to a change in

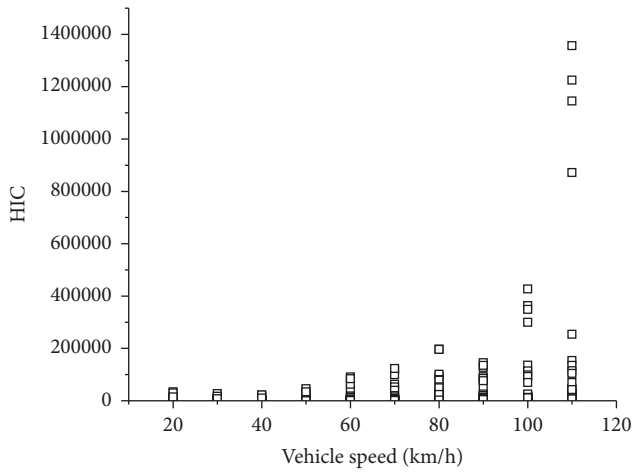

Figure 8: Relationship between vehicle speed and the HIC.

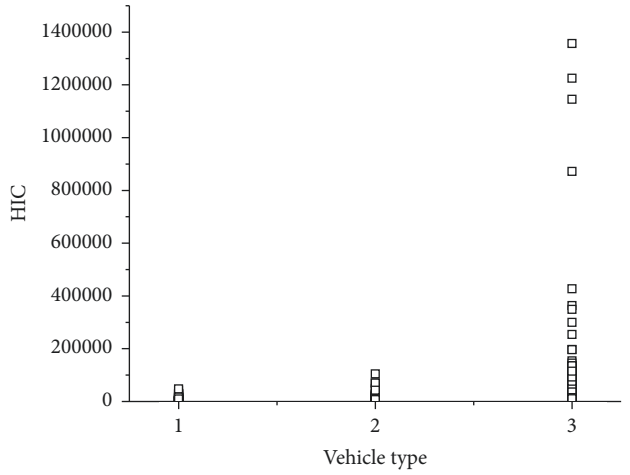

Figure 9: Relationship between vehicle model and the HIC.

collision position and pedestrian speed, which has little impact on pedestrian injury. Therefore, it will be eliminated in the later analysis.

Figures 8–10 show the relationship between significant risk factors and the HIC. Figure 8 shows that the HIC value gradually increases with increasing vehicle speed, and the increasing trend is increasingly larger. As shown in Figure 9, a flat head, high head, and short head are more likely to cause injury to the pedestrian head, while a high head and short head have the same impact on the pedestrian head. As shown in Figure 10, pedestrian injury is more serious when the collision angle is 0° than when the collision angle is 90°; that is, injury caused by a rear collision between the vehicle and the pedestrian is greater than that caused by a side collision between the vehicle and pedestrian. The analysis shows that a rear collision between cars and pedestrians easily causes pedestrians to recline, which increases the probability of a serious collision between the head and automobile engine cover, front windshield, or A-pillar.

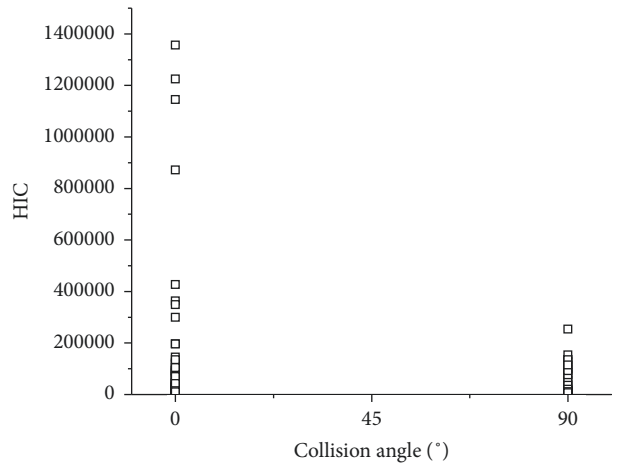

Figure 10: Relationship between impact angle and the HIC.

Table 10 shows how scholars use various methods to identify the significant risk factors based on data sources from different areas and times. Besides collision angle, the significant risk factors identified in this paper are basically consistent with those identified by other researchers, such as the vehicle speed and vehicle type. In terms of vehicle type, factors screened by other scholars, such as larger vehicles, light machinery trucks, and light passenger vehicles, all belong to the category of flat-headed vehicles identified in this paper, which indicate that the research results of this paper are not limited by region and time and have universal applicability.

With reference to the relationship between the above variables and the HIC value, the nonlinear relationship between the HIC and vehicle speed was fitted using multiple regression analysis for different vehicle types and collision angles, as shown in Table 11. According to the determination coefficient R^2 between different expressions (the greater the value is, the better the goodness of fit), the optimal relationship models of the HIC, vehicle speed, and collision angle corresponding to different models are determined as follows.

(1) Short head type:

$$\mathrm{HIC} = \frac{\theta}{90^\circ}\left(-1105.442 + 105.627V_S - 3.196V_S^2 + 0.032V_S^3\right) + \left(1 - \frac{\theta}{90^\circ}\right)\left(0.006V_S^{3.276}\right). \tag{7}$$

(2) High head type:

$$\mathrm{HIC} = \frac{\theta}{90^\circ}\left(0.0001V_S^{3.831}\right) + \left(1 - \frac{\theta}{90^\circ}\right)\left(4313.065 - 271.598V_S + 4.424V_S^2\right). \tag{8}$$

(3) Flat head type:

Table 10: Comparison of the conclusions in this paper and other research.

Literature	Method	Significant risk factor	Data source
This paper	Multiple regression analysis and correlation analysis	Vehicle speed, vehicle type (flat-headed vehicles), and collision angle (rear-end collision)	PC-Crash simulation
[18]	Multilevel model	Pedestrian age and vehicle type (larger vehicles)	Pedestrian-vehicle collision data from 2015 to 2017 in South Korea
[21]	Partial least squares discriminant analysis	Pedestrian age, pedestrian gender, vehicle type (light machinery), and accident time	Fatal pedestrian crash in Tabriz, Iran, during 2014 to 2015
[22]	Multivariate logistic regression	Vehicle speed (in excess of 40 km/h) and collision location	Pedestrian-vehicle accident cases in Chongqing, China, from 2011 to 2015
[23]	Statistical tests	Vehicle type (trucks, light passenger vehicles) and light level	Fatal pedestrian accidents of low-speed vehicles in Japan from 2005 to 2014

Table 11: Model fitting results.

Number	Model	Collision angle	Model expression	R^2
1	Short head type	$\theta = 90^\circ$	$\mathrm{HIC} = 5.195e^{0.08V_S}$	0.958
2			$\mathrm{HIC} = -1105.442 + 105.627V_S - 3.196V_S^2 + 0.032V_S^3$	0.980
3			$\mathrm{HIC} = 8.968e^{-5}V_S^{3.935}$	0.945
4		$\theta = 0^\circ$	$\mathrm{HIC} = 5.616e^{0.069V_S}$	0.941
5			$\mathrm{HIC} = e^{10.922-143.901V_S^{-1}}$	0.931
6			$\mathrm{HIC} = 0.013V_S^{3.09}$	0.905
7			$\mathrm{HIC} = 0.006V_S^{3.276}$	0.935
8			$\mathrm{HIC} = 0.002V_S^{3.552}$	0.918
9	High head type	$\theta = 90^\circ$	$\mathrm{HIC} = 7.222e^{0.071V_S}$	0.966
10			$\mathrm{HIC} = 3.344e^{0.078V_S}$	0.975
11			$\mathrm{HIC} = 0.0001V_S^{3.831}$	0.988
12		$\theta = 0^\circ$	$\mathrm{HIC} = 4.43e^{0.075V_S}$	0.969
13			$\mathrm{HIC} = 4313.065 - 271.598V_S + 4.424V_S^2$	0.934
14			$\mathrm{HIC} = -72412.624 + 5232.291V_S - 107.569V_S^20.67V_S^3$	0.920
15			$\mathrm{HIC} = 0.002V_S^{3.622}$	0.909
16			$\mathrm{HIC} = 0.002V_S^{3.608}$	0.924
17	Flat head type	$\theta = 90^\circ$	$\mathrm{HIC} = 39206.161 - 1867.829V_S + 20.139V_S^2 + 0.119V_S^3$	0.963
18			$\mathrm{HIC} = 57651.927 - 3377.693V_S + 55.218V_S^2 - 0.152V_S^3$	0.982
19			$\mathrm{HIC} = 17718.827 - 449.132V_S - 3.278V_S^2 + 0.155V_S^3$	0.984
20		$\theta = 0^\circ$	$\mathrm{HIC} = 56592.336 - 2915.804V_S + 40.36V_S^2 - 0.079V_S^3$	0.978
21			$\mathrm{HIC} = -458713.785 + 34542.659V_S - 735.559V_S^2 + 4.804V_S^3$	0.966
22			$\mathrm{HIC} = 2946.727e^{0.047V_S}$	0.910
23			$\mathrm{HIC} = -729141.994 + 54160.807V_S - 1112.044V_S^2 + 7.001V_S^3$	0.907
24			$\mathrm{HIC} = -871724.682 + 63661.079V_S - 1297.743V_S^2 + 8.087V_S^3$	0.890

$$\mathrm{HIC} = \frac{\theta}{90^\circ}\left(17718.827 - 449.132V_S - 3.278V_S^2 + 0.155V_S^3\right) + \left(1 - \frac{\theta}{90^\circ}\right)\left(-458713.785 + 34542.659V_S - 735.559V_S^2 + 4.804V_S^3\right). \tag{9}$$

5.2. Accident Risk Assessment. According to the data obtained in the tests, combined with the HIC security threshold introduced in Section 3.1, the data with $\mathrm{HIC} \le 1$ were screened out and classified as a separate group, and the risk level was determined as level I. The remaining 183 groups of data were numbered according to the HIC value from small to large, and the HIC ordered sample was generated, which was denoted as x_i ($i = 1, 2, \ldots, 183$).

According to the specific implementation steps of Fisher's optimal segmentation algorithm introduced in Section 3.2, this study uses MATLAB to write the algorithm code, calculates the class diameter and minimum error function of the HIC ordered samples, and draws the variation curve of the minimum error function with the classification number k, as shown in Figure 11.

As shown in Figure 11, when $k = 3$ and 4, the curvature of the minimum error function curve changes significantly. To further determine the optimal classification number, the minimum error function ratio $\beta(k)$ between adjacent classification numbers is calculated as shown in Table 12.

According to Table 12, $\beta(4)$ is greater than $\beta(3)$, so $k = 4$ is the optimal classification number. In addition, the classification numbers corresponding to the optimal classification of ordered samples can be obtained from Table 6, and

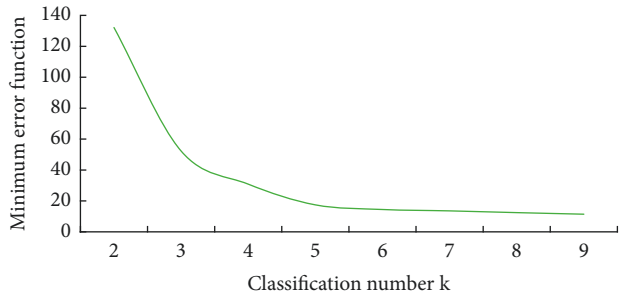

Figure 11: Relationship between the minimum error function and the classification number.

Table 12: Classification results.

k	Minimum error function	Classification	β value
2	132.125	{1~117} {118~183}	-
3	52.271	{1~117} {118~171} {172~183}	1.69
4	30.856	{1~64} {65~117} {118~171} {172~183}	1.77
5	17.451	{1~64} {65~94} {95~117} {118~171} {172~183}	-

Table 13: Risk evaluation standards for vehicle-pedestrian accidents.

Accident risk level	HTC threshold	Pedestrian injury level
Class I	≤1000	Mild or moderate
Class II	(1000, 5216]	Heavier
Class III	(5216, 20084]	Severe
Class IV	(20084, 144763]	Critical
Class V	>144763	Extreme

then the corresponding HIC index threshold can be determined. Based on the above research results in combination with the AIS injury classification standard (as shown in Table 1), the automobile and pedestrian accident risk classification evaluation method is presented, as shown in Table 13.

6. Case Analysis

To evaluate the effectiveness of the accident risk classification evaluation method proposed in this paper, 50 typical vehicle-pedestrian accidents are selected for verification (as shown in Table 14), including 20 short-head automobile accidents, 19 high-head automobile accidents, and 11 flat-head automobile accidents. First, according to the information of each accident case, combined with models (7)–(9) fitted in Section 5.1, the HIC value corresponding to each accident is calculated, and then the accident risk level is determined according to Table 13. Finally, the evaluation method of automobile pedestrian accident risk classification is verified using the actual injury level of pedestrians. Among them, the actual injury level of pedestrians is evaluated using the trauma scoring system Version 3.0 according to the injury report issued by a hospital or medical examiner.

It can be seen from the evaluation results in Table 14 that the risk level corresponding to 5 accidents calculated using the accident risk evaluation method proposed in this paper is not consistent with the actual pedestrian injury level, namely, cases 22, 30, 39, 43, and 46, with an error rate of 10%. Considering that the error rate cannot accurately measure the degree of error classification of accident risk using risk assessment methods, this paper proposes a new index to evaluate the accuracy of accident risk assessment methods, namely, the error classification degree α, as shown in formula (10). According to formula (10), the degree of error classification is 2.59%, which is within the acceptable range, thus verifying the accuracy of the risk assessment method of automobile and pedestrian accidents proposed in this paper.

$$\alpha = \frac{\sum_{i=1}^{n} \eta_{ij} \mathrm{FN}_{ij}}{\mathrm{TN} + \sum_{i=1}^{n} \eta_{ij} \mathrm{FN}_{ij}} \quad i \neq j, \tag{10}$$

where TN is the number of correctly graded cases; FN_{ij} is the number of cases of the i pedestrian injury level misclassified at the j risk level; n is the number of risk levels divided; and η_{ij} is the corresponding weight coefficient; the calculation formula is

$$\eta_{ij} = \frac{|j - i|}{n}. \tag{11}$$

The research results of this paper can not only provide a scientific judgment basis for accident analysis and treatment but also provide a reference for speed limit management. For example, in the absence of effective accident scene evidence and video surveillance, a judicial appraisal institution can determine the corresponding HIC range from Table 13 according to the pedestrian injury level in the accident. Then, combined with the car accident and collision shape, using the optimal fitting model, this research deduced the range of speed in a trouble-causing car accident, and the calculation result is helpful to a traffic police department responsible for both sides of the accident. Similarly, for sections with a high incidence of vehicle-pedestrian accidents, the maximum allowable speed that can guarantee HIC≤1000 (the accident risk is grade I) can also be deduced based on the optimal model for different models to formulate the speed management scheme.

Table 14: Case validation.

Number	Accident speed (km/h)	Collision form	Model	Actual pedestrian injury level	HIC	Accident risk level
1	75	Rear-end collision	Short head type	Severe	8334	III
2	84	Side collision	Short head type	Heavier	4183	II
3	50	Rear-end collision	Short head type	Heavier	2208	II
4	47	Side collision	Short head type	Mild	121	I
5	56	Side collision	Short head type	Moderate	407	I
6	70	Side collision	Short head type	Heavier	1604	II
7	82	Side collision	Short head type	Heavier	3710	II
8	95	Side collision	Short head type	Severe	7521	III
9	34	Rear-end collision	Short head type	Moderate	624	I
10	51	Rear-end collision	Short head type	Heavier	2356	II
11	49	Rear-end collision	Short head type	Heavier	2066	II
12	80	Rear-end collision	Short head type	Severe	10296	III
13	85	Rear-end collision	Short head type	Severe	12558	III
14	44	Side collision	Short head type	Mild	81	I
15	48	Side collision	Short head type	Mild	140	I
16	66	Side collision	Short head type	Heavier	1144	II
17	71	Rear-end collision	Short head type	Severe	6964	III
18	77	Rear-end collision	Short head type	Severe	9084	III
19	89	Side collision	Short head type	Severe	5539	III
20	40	Side collision	Short head type	Mild	54	I
21	37	Rear-end collision	High head type	Mild	320	I
22	69	Rear-end collision	High head type	Heavier	6635	III
23	76	Rear-end collision	High head type	Severe	9225	III
24	99	Rear-end collision	High head type	Critical	20784	IV
25	105	Rear-end collision	High head type	Critical	24570	IV
26	73	Rear-end collision	High head type	Severe	8062	III
27	62	Rear-end collision	High head type	Heavier	4480	II
28	55	Side collision	High head type	Moderate	465	I
29	78	Rear-end collision	High head type	Severe	10044	III
30	74	Side collision	High head type	Severe	1449	II
31	55	Side collision	High head type	Moderate	465	I
32	53	Side collision	High head type	Moderate	403	I
33	30	Side collision	High head type	Mild	46	I
34	50	Side collision	High head type	Moderate	323	I
35	47	Rear-end collision	High head type	Heavier	1321	II
36	49	Rear-end collision	High head type	Heavier	1627	II
37	51	Side collision	High head type	Moderate	348	I
38	63	Side collision	High head type	Moderate	782	I
39	65	Side collision	High head type	Heavier	882	I
40	76	Rear-end collision	Flat head type	Critical	26780	IV
41	72	Side collision	Flat head type	Extreme	186242	V
42	58	Side collision	Flat head type	Extreme	170884	V
43	48	Side collision	Flat head type	Severe	165750	V
44	69	Side collision	Flat head type	Extreme	182041	V
45	78	Side collision	Flat head type	Extreme	196299	V
46	34	Rear-end collision	Flat head type	Severe	54247	IV
47	83	Rear-end collision	Flat head type	Critical	87926	IV
48	88	Rear-end collision	Flat head type	Extreme	158663	V
49	97	Rear-end collision	Flat head type	Extreme	355531	V
50	77	Rear-end collision	Flat head type	Critical	33126	IV

In addition, because the collision between an automobile hood and pedestrians easily causes fatal injuries, the space between the hood and various parts in the engine compartment can be considered in the design of a vehicle to ensure that the hood has enough deformation space for cushioning the impact force. Of course, improving active safety technology and road design will also play a role in protecting pedestrians. For example, by capturing the movement characteristics of pedestrians and vehicles, computer vision technology can be used to predict potential accidents between pedestrians and vehicles at signalized intersections, which can be used for the development of collision warning systems in connected vehicle environments [28].

7. Conclusion

Based on accident case investigations, this research uses PC-Crash to carry out vehicle-pedestrian collision simulation tests under different accident patterns, revealing the significant risk factors (i.e., vehicle speed, collision angle, and vehicle type) affecting pedestrian injury. For different vehicle types, a multivariate relationship model between the HIC, vehicle speed, and collision angle is built, and a classification evaluation method of vehicle-person accident risk based on the HIC is proposed and verified. Research results of this paper can promote pedestrian injury reduction in accidents and provide guidance on speed limit measures.

Although this research has made some innovative achievements, there are still the following deficiencies. For example, this paper only selects Chinese 90^{th}% adult men as representatives for the crash tests, without considering adult women, children, the elderly, and other groups. As a result, the factors involved in the proposed accident risk evaluation method are not sufficiently comprehensive and ignore factors of pedestrian gender or pedestrian age that may affect the accident risk. In addition, the values of the variables were relatively low in the test process, and there was no relevant research on occupant movement. Therefore, follow-up research work can consider increasing the value range of variables and combining PC-Crash and MADYMO software to conduct in-depth research on the injury mechanisms of different pedestrian groups and the response of drivers in the car before and after the accident.

Data Availability

The data used to support the findings of this study are available from the corresponding author upon request.

Conflicts of Interest

The authors declare that they have no conflicts of interest.

Acknowledgments

This study was supported by the National Nature Science Foundation of Guangxi Province (Nos. 2022GXNSFBA035640, 2019GXNSFBA245050, and 2019JJB160047), the Guangxi University Young and Middle-aged Teachers Scientific Research Basic Ability Improvement Project (2022KY0193), the Guangxi Science and Technology Base and Talent Special Project (Nos. AD20159035 and AD22035153), and the Fund for Less-developed Regions of the National Natural Science Foundation of China (No. 71861006).

References

[1] Traffic Management Bureau of the Ministry of Public Security, *Road Traffic Accident Statistical Annual Report*, OECD, Beijing, China, 2021.

[2] H. Pritz, C. Hassler, J. Herridge, and E. Weis, "Experimental study of pedestrian injury minimization through vehicle design," in *Proceedings of the 19 Th Stapp Car Crash Conference*, pp. 725–751, SAE Warrendale PA, California, USA, November 1975.

[3] H. Cheng and A. L. Rizer, *Articulated Total Body Model Version V User's Manual*, pp. 637–648, United States Air Force Research Laboratory, USA, 1998.

[4] R. R. Mchenry, "Analysis of the dynamics of automobile passenger restraint systems," in *Proceedings of the 7th Stapp Car Crash Conference*, pp. 420–431, California, USA, 1963.

[5] H. Appel, G. Sturtz, and L. Gotzen, "Influence of impact speed and vehicle parameter on injuries of children and adults in pedestrian accidents," in *Proceedings of the 2nd IRCOBI Conference*, pp. 83–100, Hong Kong, China, September 1975.

[6] D. Severy and H. Brink, "Auto-pedestrian collision experiments," *SAE Transactions*, vol. 75, pp. 323–371, 1967.

[7] Y. Matsui, H. Ishikawa, and A. Sasaki, "Proposal of injury risk curves for evaluating pedestrian femur/pelvis injury risk using EEVC upper legform impactor based on accident reconstruction," *International Journal of Crashworthiness*, vol. 11, no. 2, pp. 97–104, 2006.

[8] R. Cheng, Y. Pan, and T. Wang, "A design method for the roadside clear zone based on accident simulation analysis," *Mathematical Problems in Engineering*, vol. 202116 pages, Article ID 2605095, 2021.

[9] G. Cheng, R. Cheng, Y. Pei, and L. Xu, "Probability of roadside accidents for curved sections on highways," *Mathematical Problems in Engineering*, vol. 2020, Article ID 9656434, 18 pages, 2020.

[10] J. Mandelík and M. Bundzel, "Application of neural network in order to recognise individuality of course of vehicle and pedestrian body contacts during accidents," *International Journal of Crashworthiness*, vol. 24, no. 2, pp. 221–234, 2019.

[11] S. Xu, X. Jin, C. Qin, and X. Chai, "Personalized customization method of hybrid human model for pedestrian-vehicle accident reconstruction," *Journal of Mechanics in Medicine and Biology*, vol. 21, no. 02, Article ID 2150009, 2021.

[12] D. Grindle, W. Pak, B. Guleyupoglu et al., "A detailed finite element model of a mid-sized male for the investigation of traffic pedestrian accidents," *Proceedings of the Institution of Mechanical Engineers - Part H: Journal of Engineering in Medicine*, vol. 235, no. 3, pp. 300–313, 2021.

[13] P. Panday, A. Vikram, A. Chawla, and S. Mukherjee, "Prediction of lower extremity injuries in car-pedestrian crashes – real-world accident study," *Traffic Injury Prevention*, vol. 22, no. 2, pp. 173–176, 2021.

[14] M. Lalwala, A. Chawla, P. Thomas, and S. Mukherjee, "Finite element reconstruction of real-world pedestrian accidents using thums pedestrian model," *International Journal of Crashworthiness*, vol. 25, no. 4, pp. 360–375, 2020.

[15] S. Zhu, "Analyse vehicle–pedestrian crash severity at intersection with data mining techniques," *International Journal of Crashworthiness*, vol. 5, no. 26, pp. 1–9, 2021.

[16] A. Sheykhfard, F. Haghighi, T. Nordfjærn, and M. Soltaninejad, "Structural equation modelling of potential risk factors for pedestrian accidents in rural and urban roads," *International Journal of Injury Control and Safety Promotion*, vol. 28, no. 1, pp. 46–57, 2021.

[17] N. Kamboozia, M. Ameri, and S. M. Hosseinian, "Statistical analysis and accident prediction models leading to pedestrian injuries and deaths on rural roads in Iran," *International Journal of Injury Control and Safety Promotion*, vol. 27, no. 4, pp. 493–509, 2020.

[18] S. Park and D. Ko, "A multilevel model approach for investigating individual accident characteristics and neighborhood environment characteristics affecting pedestrian-vehicle

crashes," *International Journal of Environmental Research and Public Health*, vol. 17, no. 9, p. 3107, 2020.

[19] D. Lasota, A. Al-Wathinani, P. Krajewski, K. Goniewicz, and W. Pawlowski, "Alcohol and road accidents involving pedestrians as unprotected road users," *International Journal of Environmental Research and Public Health*, vol. 17, no. 23, pp. 8995–95, 2020.

[20] J. Hasani, S. Erfanpoor, A. Rajabi et al., "Spatial analysis of mortality rate of pedestrian accidents in Iran during 2012–2013," *Traffic Injury Prevention*, vol. 20, no. 6, pp. 636–640, 2019.

[21] M. Jamali-Dolatabad, H. Sadeghi-Bazargani, and P. Sarbakhsh, "Predictors of fatal outcomes in pedestrian accidents in Tabriz Metropolis of Iran: application of pls-da method," *Traffic Injury Prevention*, vol. 20, no. 8, pp. 873–879, 2019.

[22] C. Feng, A. Duan, J. Qiu et al., "Investigation of head injuries suffered by pedestrians in traffic accidents via videos," *International Journal of Crashworthiness*, vol. 25, no. 6, pp. 680–688, 2020.

[23] Y. Matsui and S. Oikawa, "Situational characteristics of fatal pedestrian accidents involving vehicles traveling at low speeds in Japan," *Traffic Injury Prevention*, vol. 20, no. sup1, pp. 1–6, 2019.

[24] Editorial Department of China Journal of Highway and Transport, "Review on China's automotive engineering research process: 2017," *China Journal of Highway and Transport*, vol. 30, no. 6, pp. 1–197, 2017.

[25] G. Cheng, R. Cheng, Y. Pei, L. Xu, and W. Qi, "Severity assessment of accidents involving roadside trees based on occupant injury analysis," *PLoS One*, vol. 15, no. 4, Article ID e0231030, 2020.

[26] G. Cheng, R. Cheng, L. Xu, and W. Zhang, "Risk assessment of roadside accidents based on occupant injuries analysis," *Journal of Jilin University (Engineering and Technology Edition)*, vol. 51, no. 3, pp. 875–885, 2021.

[27] D. Liu, Y. Li, H. Zhao, and X. Zhu, "Relativity analysis of pedestrian head injuries and the headform to bonnet top test method," *Journal of Highway and Transportation Research and Development*, vol. 2004, no. 1, pp. 98–101, 2004.

[28] S. Zhang, M. Abdel-Aty, Y. Wu, and O. Zheng, "Modeling pedestrians' near-accident events at signalized intersections using gated recurrent unit (GRU)," *Accident Analysis & Prevention*, vol. 148, Article ID 105844, 2020.